Strain shadow “megapores” in mid-crustal ultramylonites

Florian Fusseis[1], Craig Allsop[2], James Gilgannon[1], Christoph Schrank[3], Simon Harley[1], Christian M. Schlepütz[4]

[1]School of Geosciences, The University of Edinburgh, EH9 3FE, UK

[2] Civil and Environmental Engineering, James Weir Building, Strathclyde University, G1 1XJ UK

[3] School of Earth & Atmospheric Sciences, Queensland University of Technology, St Lucia QLD 4067, Brisbane, Australia

[4] Swiss Light Source, Paul-Scherrer Institute, Forschungsstrasse 111, 5232 Villigen, Switzerland

ABSTRACT

Mylonitic shear zones are important fluid-conduits in the Earth’s crust. They host transient and permeable porosity that facilitates fluid transfer and controls fluid-rock interaction. Here we present microstructural observations from a mid-crustal ultramylonite with very large pores that occupy the strain shadows of albite porphyroclasts. Our non-invasive 3D X-ray microtomographic data show that the largest of these strain shadow megapores have substantial volumes of up to ~$1.7x10^5$ µm³. As the sample shows no signs of retrogressive overprint or weathering, these pores must be synkinematic. Importantly, the close proximity of the pores to creep cavities in dynamically recrystallized quartz ribbon grains suggests a potential hydraulic link between fluid in the strain shadow megapores and fluid in the creeping rock matrix. The evolving megapores constitute very large syn-deformational local fluid reservoirs in mylonites that likely fed into the granular fluid pump established by the dynamically evolving creep cavities. Our findings add to an emerging picture of the dynamic transport properties of ultramylonitic shear zones, where the formation and destruction of porosity are intrinsically

This is a peer-reviewed, accepted author manuscript of the following article: Fusseis, F., Allsop, C., Gilgannon, J., Schrank, C., Harley, S., & Schlepütz, C. M. (2023). Strain shadow "megapores" in mid-crustal ultramylonites. Geology, 51(8), 748-752. https://doi.org/10.1130/g51128.1

linked to microscale deformation processes. They also suggest that despite many studies on porphyroclast systems, open questions remain, especially concerning the interaction of clasts with their matrix.

SHEAR ZONE AND ULTRAMYLONITE

Exhumed shear zones allow studying processes that govern the behaviour of plate boundaries at depth. One of these processes is fluid migration. We know that shear zones are the primary crustal fluid conduits (e.g. Carter and Dworkin, 1990; Menegon et al., 2015; Putnis, 2021). Fluid pathways in mylonitic shear zones include grain boundaries and various types of synkinematic porosity (e.g. Hay et al., 1988; Wark & Watson, 2000; Ingebritsen & Manning, 2010; Fusseis et al., 2009). Mechanisms that generate porosity in mylonites include reactive volume change, dissolution and creep cavitation (e.g. Putnis, 2021; Fusseis et al., 2009). Before the advent of non-invasive imaging techniques studying these pores in deformed rocks has been difficult, and a comprehensive understanding of synkinematic porosity and fluid transport in mylonitic shear zones is thus still missing.

To better understand the processes that produce porosity in mid-crustal ultramylonites, we investigated a fresh sample from the northern Cap de Creus peninsula, NE Spain. There, shear zone networks formed under retrograde, greenschist facies metamorphic conditions in a transpressive strike-slip setting (Carreras, 2001, Druguet, 2001). In the study area, deformation was simple-shear dominated (Fusseis et al., 2006).

Shear zone networking in the Cala Serena area involved the formation of highly-deformed mm-cm wide ultramylonitic sheets with high lateral strain gradients (Fig. 1). These sheets formed predominantly by reaction weakening, which included the compositional adjustment of a high-temperature biotite to greenschist-facies conditions via $Bt_1 \rightarrow Bt_2+Ms_2+Chl+Ilm$[1] (Kerrich et al.,

1 Mineral abbreviations after Whitney and Evans, 2010, American Mineralogist, v. 95, 185–187.

1980), as well as the consumption of Ab_1 in the formation of Ab_2, Ap and Grt (see Fusseis, 2006, for details). Both reactions contributed to the formation of a fine-grained (< 15 µm), polyphase matrix composed of Qtz_2, Bt_2, Ab_2, Ms_2, with accessory Ilm, Mag, Chl, Grt and Ap (Fig. 2a). Within the matrix, the basal planes of Bt_2, a large number of aligned phase boundaries as well as Ilm needles define a mylonitic foliation S_m. Fusseis & Handy (2008) infer the dominant deformation mechanism in the matrix to have been viscous grain boundary sliding (VGBS), assisted by pressure solution and the precipitation of secondary mineral phases from a fluid via preferential heterogeneous nucleation. The polyphase matrix is segmented by monomineralic ribbon grains formed by Qt_1, now dynamically recrystallized to Qtz_2 (recrystallized grain size < 70 µm, Fig. 2). Qtz_2 in the ribbon grains formed by subgrain rotation and minor grain boundary bulging (Fusseis & Handy, 2008) and shows no evidence for static recrystallization. The quartz ribbons are not boudinaged and exhibit creep cavities similar to those described by Gilgannon et al. (2017) (Fig. 2b and supplementary video 1).

PORPHYROCLASTS

The ultramylonite exhibits numerous porphyroclasts, most of which are albitic plagioclase (Ab_1), with significantly fewer Ms_1 and rare Bt_1 (Suppl. Video 1). These clasts are inherited from the psammitic host rock (Suppl. Fig. 1). We focus on the Ab_1 porphyroclasts, which appear smaller in the ultramylonite: In the host rock they have mean long axes of 208±59 µm, whereas in the ultramylonites these are 130±55 µm (Supp. Fig. 3b, e). The size difference and the absence of core-mantle structures indicate that, during mylonitization, the clasts dissolved (Fusseis, 2006). While some clasts show intragranular fractures that terminate at the grain boundaries, no obvious internal dissolution channels were observed, which suggests that grain size reduction happened

preferentially on the outer interfaces of Ab_1 with the matrix. Locally, increased porosity and small secondary grains at these interfaces support this interpretation.

In the XZ plane of finite strain many clasts appear asymmetric (aspect ratio 1.61±0.29, compared with 1.51±0.34 in the host rock, see supplementary Fig. 3a and d) and inclined with respect to the shear plane, with the long-axes orientation distributions showing two maxima: a majority of clasts are inclined with an angle α between 20 and 60° against the shear plane (measured synthetically from S_m), fewer at 130 to 170° (Suppl. Fig. 3c). The strain shadows of the Ab_1 porphyroclasts are defined either by Bt_2 grains, or pores (Fig. 2, Suppl. videos 2-5).

S_m wraps around the Ab_1 porphyroclasts producing asymmetric distortion patterns that indicate clast rotation (Suppl. Fig. 2). The perturbations of S_m are much more subtle than those predicted by numerical studies (e.g., Samanta et al., 2002) but this is likely determined by the comparatively large matrix grain size.

STRAIN SHADOW MEGAPORES (SSMPs)

About a third of Ab_1 porphyroclasts exhibit pores in one of two habits in their immediate vicinity: either a cluster of smaller pores, or large, isolated pores (Fig. 3, Suppl. Videos). Often, the pores mimic the shapes of what would be sigmoidal strain shadows with stair stepping (Fig. 2, Suppl. Videos). Some of the pores exhibit evidence for mineral precipitation (often Mag, Suppl. Figs. 2c, d), but many are free of precipitates. Others seem to contain remnants of dissolved Bt. Our non-invasive 3-dimensional x-ray microtomographic data show that the pores appear, to the level of resolution, isolated and unconnected to any potential postmylonitic fluid pathways. Ab_1 porphyroclasts in the unsheared host rock do not exhibit these pores (Suppl. Fig. 1).

From the µCT data, we analysed 73 Ab_1 SSMPs with volumes over 6591 µm³ (3000 voxels). We recorded the position of each pore with respect to the clast, the pore volume, the clast size, clast aspect ratio and its long axis orientation. The analysis (Fig. 4) shows that the majority of SSMPs have volumes between $1x10^4$ and $1x10^5$ µm³. The largest pore has a volume of ~$1.7x10^5$ µm³. Pores form asymmetrically about the shear plane around clasts that are, on average 115±51 µm long. More pores (n=40) form at the top SE side of the clasts than at the bottom NW side (n=32). These are in the locations of the clasts' expected strain shadows. Only one pore formed at the top NW side in a location that often exhibits newly grown Mag. Pores occur around clasts with a range of aspect ratios and long axis orientations. More pores occur around clasts with a low α than clasts with a high α. There is a weak link between clast orientation and pore volume, with pores around clasts with low α seemingly having a greater volume.

DISCUSSION

Pores can exist as robust features in rocks even at great depth (Walsh, 1965, Christensen, 1974), but inevitably they will evolve with their host rock. We interpret the SSMPs as a form of synkinematic porosity (see suppl. Material for arguments). As such, pore formation should be linked to the behavior of the porphyroclasts and their interaction with the matrix and any fluids in the system (Marques et al., 2014). No simple model explains the formation of SSMPs, but we can constrain the coupled mechanical, chemical and hydraulic processes that will likely have contributed: 1) dilatancy in the strain shadows around porphyroclasts, 2) local chemical disequilibria between the fluid and the matrix that facilitate dissolution, 3) detachments at the clast/matrix interface, and 4) viscous granular flow with diverging flow trajectories in the ultramylonitic matrix. While our data do currently not allow us to determine the relative

113 contributions of these mechanisms, we can constrain the likely circumstances of SSMP
114 formation:
115 1) Strain shadows are sites of tectonic underpressure, where the pore fluid factor λ_v will approach
116 1 and the rock can dilate (Mancktelow, 2008). This dilation leads to the formation of fibrous vein
117 fillings and strain fringes (e.g., Cox & Etheridge, 1989, Koehn et al., 2000) and should be
118 responsible for the vein formation in the strain shadow of a rigid spherical inclusion in a
119 viscously deforming crystalline matrix described by Marques and Burlini (2008). We expect
120 transient pressure variations around porphyroclasts to play a role in SSMP formation.
121 2) Where transient dilatancy facilitates fluid ingress, a chemical disequilibrium between the fluid
122 and its host minerals may lead to dissolution or precipitation of new minerals (e.g., Kruse &
123 Stünitz, 1999, Kenkmann, 2000). In some pores, Bt sheets appear as remnants of larger dissolved
124 grains, in others Mag forms newly precipitated coatings, and many porphyroclasts show intact
125 Bt_2 in their strain shadows indicating that precipitation dominated locally. However, chemical
126 disequilibria may be locally controlled and open porosity found around porphyroclasts implies
127 that fluid ingress seems possible without subsequent mineral precipitation, similar to creep
128 cavities.
129 3) Porphyroclasts can experience systematic detachments at the clast/matrix interface in spatial
130 domains where a majority of SSMPs in our sample occur (Samanta and Battacharaya, 2003).
131 According to these authors, detachments normal and/or parallel to the interface occur where the
132 adhesive strength of coherence between the inclusion and matrix is exceeded. The distribution of
133 these displacements along the interface is a function of the aspect ratio and orientation of the
134 clast, and must evolve as a clast rotates. We see evidence for both rotation and detachments in
135 our sample: Clast rotation during shearing is indicated by the perturbed foliations around Ab_1

porphyroclasts (Fig. 2 and supplementary Fig. 2, cf. Samanta et al., 2003), and some SSMPs could be interpreted to be the result of detachments between a rotating clast and the matrix (Suppl. Fig. 2b).

Furthermore, our measurements indicate that the clasts shrink (Suppl. Fig. 3). Shrinkage likely occurred by dissolution in a grain boundary fluid, potentially accelerated along the highly stressed parts of their interfaces with the matrix, which would explain the observed increase in the porphyroclasts' average aspect ratio. Dissolution at the clast-matrix interface should have facilitated a degree of lubrication and decoupling between the Ab_1 porphyroclasts and the matrix, potentially supporting detachments as predicted by Samanta and Battacharaya (2003).

4) The flow trajectories of individual matrix grains involved in VGBS will respond to the presence of porphyroclasts. Bjornerud (1989) and Samanta et al. (2003) modelled flow perturbations in a linearly viscous matrix around porphyroclasts and indicated diverging flow paths in strain shadows. The matrix rheology assumed in these models is unlikely to capture the complexity of the ultramylonitic matrix in our sample. However, where, as the models suggest, the movement vectors of individual matrix grains diverged due to a flow perturbation around a porphyroclast, this would have encouraged creep cavitation that may have contributed to the formation of SSMPs.

The variety of pore shapes observed in our µCT data (Suppl. Videos 1-4) and the increased porosity in the vicinity of Ab_1 porphyroclasts indicates that SSMPs evolve synkinematically and must thus be considered transient phenomena, with opening being countered by closure. The synkinematic closure of SSMPs should have been achieved by pore collapse as a consequence of VGBS and the precipitation of secondary mineral phases.

What do SSMPs mean for ultramylonitic deformation?

In mid-crustal shear zones, fluid rock interaction and fluid migration are controlled on the grain scale by a synkinematic porosity that evolves dynamically along with the ultramylonitic fabric (e.g., Fusseis et al., 2009, Menegon et al., 2015, Gilgannon et al., 2017, 2021, Précigout et al. 2019). In order to remain open at depth, all synkinematic porosity in shear zones must be filled with fluid that is more or less at lithostatic pressures throughout the life-time of the pores (e.g. Sibson, 1992; Ingebritsen et al., 2010). This must hold for the two dominant forms of synkinematic pores in the ultramylonite, the SSMPs and the creep cavities. We infer that, on the scale of the ultramylonite, the transience of both forms of porosity defines the environment in which fluids move and interact with the rock. The observation that there are a lot of small (< 6591 μm^3) pores in the vicinity of Ab_1 porphyroclasts (Fig. 2) may reflect SSMPs in various stages of their development and may thus be an expression of this transience. Since pore sizes must be expected to evolve dynamically, the amount of fluid stored in pores must vary, with fluid gained during pore opening and fluid lost during closing. As they reach substantial volumes, the SSMPs constitute significant, temporary local fluid reservoirs. These reservoirs could interact with fluids that would have been stored and transported in the creep cavities by the action of the granular fluid pump, which has been postulated to drive a dynamic transfer of fluids and dissolved chemical components (Fusseis et al., 2009). We infer the synkinematic transport properties of the shear zone to have been defined by the combined evolution of SSMPs and creep cavities. As both porosities result from complex hydraulic-chemical-mechanical interactions and feedbacks, the formation and destruction of synkinematic porosity must thus be considered as an important energy dissipation mechanism in reacting and deforming rocks and integral to processes in mid-crustal shear zones.

Implications

Should we expect SSMPS elsewhere, and are they even a common feature in mylonites? Porphyroclast systems have been described across the crust and even in mantle shear zones, and the processes we discuss above apply to all of them. While this is the first formal description of SSMPs, they might thus have been overlooked elsewhere. µCT imaging enables non-invasive insight into microstructures and thus a novel perspective. Were the technique applied to other ultramlyonitic samples, SSMPs would possibly be found more frequently.

If SSMPs are present in all mylonites with porphyroclasts then they will, alongside creep cavities and other forms of synkinematic porosity, contribute to complex spatially and temporally heterogeneous fluid pathways in these rocks. These pathways will dominate where fluid-rock interaction occurs and this will impact if and where mineral reactions proceed. This notion is reinforced by recent observations of heterogeneous fluid pathways in mylonites (Bestmann et al., 2021) and metamorphic rocks (e.g. Konrad-Schmolke & Halama, 2014, Beinlich et al., 2020). Classic thermodynamic considerations of mineral stability in mylonites would not account for such extreme spatial and temporal variations of mass flux. The effects of dynamic transport in shear zones may be better understood by invoking research on reactive transport (e.g. Beinlich et al., 2020). Ultimately, we are inching towards a more holistic understanding of the transport properties of ultramylonitic shear zones and thus towards better models for fluid transfer across the crust.

REFERENCES CITED

Beinlich, A., John, T., Vrijmoed, J. C., Tominaga, M., Magna, T., and Podladchikov, Y. Y., 2020, Instantaneous rock transformations in the deep crust driven by reactive fluid flow. Nature Geoscience, v. 13(4), 307-311.

Bestmann, M., Pennacchioni, G., Grasemann, B., Huet, B., Jones, M. W., and Kewish, C. M., 2021, Influence of Deformation and Fluids on Ti Exchange in Natural Quartz. Journal of Geophysical Research: Solid Earth, v. 126(12), e2021JB022548.

Bjornerud, M., 1989, Mathematical model for folding of layering near rigid objects in shear deformation. Journal of Structural Geology, v. 11(3), 245-254.

Carreras, J., 2001, Zooming on Northern Cap de Creus shear zones. Journal of Structural Geology, v. 23(9), 1457-1486.

Carter, K. E., and Dworkin, S. I., 1990, Channelized fluid flow through shear zones during fluid-enhanced dynamic recrystallization, Northern Apennines, Italy. Geology, v. 18(8), 720-723.

Christensen, N. I., 1974, Compression wave velocities in possible mantle rocks to pressures of 30 Kilobars. Journal of Geophysical Research 79(2), 407-412.

Cox, S. F., and Etheridge, M. A., 1989, Coupled grain-scale dilatancy and mass transfer during deformation at high fluid pressures: examples from Mount Lyell, Tasmania. Journal of Structural Geology, v. 11(1-2), 147-162.

Druguet, E., 2001, Development of high thermal gradients by coeval transpression and magmatism during the Variscan orogeny: insights from the Cap de Creus (Eastern Pyrenees). Tectonophysics, v. 332(1-2), 275-293.

Ferry, J.M., 1985, Hydrothermal alteration of Tertiary igneous rocks from the Isle of Skye, northwest Scotland. II. Granites. Contrib. Mineral. Petrol., v. 91, 283-304.

Fusseis, F., 2006, Strain localization and shear zone formation at the brittle-viscous transition, Cap de Creus, Spain (Doctoral dissertation). Freie Universität Berlin.

Fusseis, F., Handy, M.R., Schrank, C., 2006, Networking of shear zones at the brittle-to-viscous transition (Cap de Creus, NE Spain). Journal of Structural Geology, v. 28/7, 1228-1243.

Fusseis, F., Handy, M.R., 2008, Micromechanisms of shear zone propagation at the brittle-viscous transition. Journal of Structural Geology, v. 30/10, 1242-1253.

Gilgannon, J., Fusseis, F., Menegon, L., Regenauer-Lieb, K., and Buckmann, J., 2017, Hierarchical creep cavity formation in an ultramylonite and implications for phase mixing. Solid Earth, v. 8, 1193-1209.

Gilgannon, J., Waldvogel, M., Poulet, T., Fusseis, F., Berger, A., Barnhoorn, A., and Herwegh, M., 2021, Experimental evidence that viscous shear zones generate periodic pore sheets. Solid Earth, v. 12(2), 405-420.

Konrad-Schmolke, M., and Halama, R., 2014, Combined thermodynamic–geochemical modeling in metamorphic geology: boron as tracer of fluid–rock interaction. Lithos, v. 208, 393-414.

Hay, S. J., Hall, J., Simmons, G., and Russell, M. J., 1988, Sealed microcracks in the Lewisian of NW Scotland: a record of 2 billion years of fluid circulation. J. Geol. Soc., v. 145(5), 819-830.

Ingebritsen, S. E., and Manning, C. E., 2010, Permeability of the continental crust: dynamic variations inferred from seismicity and metamorphism. Geofluids, v. 10(1-2), 193-205.

Kenkmann, T., 2000, Processes controlling the shrinkage of porphyroclasts in gabbroic shear zones. Journal of Structural Geology, v. 22(4), 471-487.

Kerrich, R., Allison, I., Barnett, R. L., Moss, S. and Starkey, J., 1980, Microstructural and Chemical-Transformations Accompanying Deformation of Granite in a Shear Zone at Mieville, Switzerland - with Implications for Stress-Corrosion Cracking and Superplastic Flow. Contributions to Mineralogy and Petrology, v. 73(3), 221-242.

Koehn, D., Hilgers, C., Bons, P. D., and Passchier, C. W., 2000, Numerical simulation of fibre growth in antitaxial strain fringes. Journal of Structural Geology, v. 22(9), 1311-1324.

Kruse, R., and Stünitz, H., 1999, Deformation mechanisms and phase distribution in mafic high-temperature mylonites from the Jotun Nappe, southern Norway. Tectonophysics, v. 303(1-4), 223-249.

Mancktelow, N. S., 2008, Tectonic pressure: Theoretical concepts and modelled examples. Lithos, v. 103(1-2), 149-177.

Marques, F. O., Burlini, L., 2008, Rigid inclusions rotate in geologic materials as shown by torsion experiments. Journal of Structural Geology, v. 30, 1368–1371.

Marques, F. O., Mandal, N., Taborda, R., Antunes, J. V., and Bose, S., 2014, The behaviour of deformable and non-deformable inclusions in viscous flow. Earth-Science Reviews, v. 134, 16-69.

Menegon, L., Fusseis, F., Stünitz, H., and Xiao, X., 2015, Creep cavitation bands control porosity and fluid flow in lower crustal shear zones. Geology, v. 43(3), 227-230.

Meunier, A., Sardini, P., Robinet, J. C., and Prêt, D., 2007, The petrography of weathering processes: facts and outlooks. Clay Minerals, v. 42(4), 415-435.

Précigout, J., Stünitz, H., and Villeneuve, J., 2019, Excess water storage induced by viscous strain localization during high-pressure shear experiment. Scientific Reports, v. 9(1), 1-9.

Putnis, A., 2021, Fluid–Mineral Interactions: Controlling Coupled Mechanisms of Reaction, Mass Transfer and Deformation. Journal of Petrology, v. 62(12), egab092.

Samanta, S.K., Bhattacharyya, G., 2003, Modes of detachment at the inclusion–matrix interface. Journal of Structural Geology, v. 25, 1107–1120.

Samanta, S.K., Mandal, N., Chakraborty, C., 2002, Development of structures under the influence of heterogeneous flow field around rigid inclusions: insights from theoretical and numerical models. Earth Science Reviews, v. 58, 85–119.

Samanta, S.K., Mandal, N., Chakraborty, C., 2003, Flow patterns around rigid inclusions in a multiple inclusion system undergoing bulk simple shear deformation. Journal of Structural Geology, v. 25, 209–221.

Sibson, R. H., 1992, Fault-valve behavior and the hydrostatic-lithostatic fluid pressure interface. Earth Science Reviews, v. 32(1-2), 141-144.

Walsh, J. B., 1965, The effect of cracks on the compressibility of rock. Journal of Geophysical Research 70(2), 381-389.

Wark, D. A., and Watson, E. B., 2000, Effect of grain size on the distribution and transport of deep-seated fluids and melts. Geophysical Research Letters, v. 27(14), 2029-2032.

Wilson, M.J., 2004, Weathering of the primary rock-forming minerals: processes, products and rates. Clay Minerals, v. 39, 233-266.

CAPTIONS

Figure 1. A: The ultramylonitic shear zone in the Cala Serena area of the Cap de Creus (NE Spain). View towards the S. UTM 31T 0521757 4686818. Sm 076/46, Ls 348/01. B: Detail of high strain fabric. C: Thin section of ultramylonite cut perpendicular to Sm and parallel to Ls (white boxes are locations of supplementary figures).

Figure 2. A: SEM image mosaic showing Ab_1 porphyroclasts floating in a polyphase ultramylonitic matrix with interspersed Qtz_2 ribbon bands. B: Map of the ultramylonite showing the x-ray attenuation of the least attenuating voxel for each XY position along a 9.75 µm long ray path orthogonal to the image plane. Pores appear black (see arrows). This visualisation technique highlights even small creep cavities in qtz ribbon grains (white arrow).

294 **Figure 3.** 3-dimensional renderings of the largest pores (> 6591 µm³ or 3000 voxels) around Ab_1
295 porphyroclasts based on the µCT data. The colours identify individual pores, the grey values
296 correspond to x-ray attenuation on a central slice through the porphyroclast.
297 **Figure 4.** Analysis of 73 strain shadow megapores. Shown are the pore volumes, their position
298 with respect to the clast (colour coding) versus associated clast long axis length. The symbols are
299 coded for aspect ratios and long axis orientation of their host clasts. Empty symbols are pores
300 that sit in between two neighbouring clasts; their position colour coding relates to the larger clast.

Supplementary Material

A synkinematic origin of the SSMPs?

Interpreting the origin of SSMPs requires the establishment of the timing of their formation: are they synkinematic or post-kinematic? Hypothetically, a younger deformational and/or metamorphic overprint, weathering or sample-preparation could have altered the sample after the mylonitic deformation. We found no evidence for either of these:

- The mylonitic deformation was the last pervasive deformation event affecting the rocks in the Cala Serena (Carreras, 2001, Fusseis et al., 2006).
- The sample shows no obvious signs of retrogression, disintegration or weathering, for which Bt and feldspars would be excellent indicators. Bt reacts to Chl and Ab during retrogression (Ferry, 1985) and weathers to Vrm or Kln (Wilson, 2004). Both Bt generations in the sample appear stable and neither Chl nor any clay minerals were found in any significant quantities. Secondary Ab is abundant in the sample, but is associated with the synkinematic consumption of Ab1. Where Ab weathers, it forms Sme, halloysite and Kln, often via internal dissolution of feldspars, and occasionally via the formation of a rim depleted in cations (Wilson, 2004), neither of which were found around Ab1 clasts, nor were clay minerals found anywhere in the sample.
- In weathering, access to meteoric water via a percolating network of pores and fractures is critical (Meunier et al., 2007). No such network exists in the sample. Our µCT data, which image the pores in a non-invasive, non-destructive way, demonstrate that the SSMPs appear isolated and are generally not connected to any postmylonitic fractures or other potential fluid pathways that could have facilitated the dissolution and selective

leaching of minerals from specific strain shadows. The non-invasive imaging also precludes that sample preparation caused the observed porosity.

- The compositionally very similar host rock in the immediate proximity of the shear zone (<1 m away), which shows no mylonitic overprint but would have experienced the same retrogression and weathering, does not exhibit SSMPs (Suppl. Fig. 1).

These arguments allow us to interpret the SSMPs in the synkinematic context of the processes that define the ultramylonite.

Ferry, J.M., 1985, Hydrothermal alteration of Tertiary igneous rocks from the Isle of Skye, northwest Scotland: II. Granites: Contributions to Mineralogy and Petrology, v. 91, p. 283–304, https://doi.org/10.1007/BF00413353.

Meunier, A., Sardini, P., Robinet, J.C., and Prêt, D., 2007, The petrography of weathering processes: Facts and outlooks: Clay Minerals, v. 42, p. 415–435, https://doi.org/10.1180/claymin.2007.042.4.01.

Wilson, M.J., 2004, Weathering of the primary rock-forming minerals: Processes, products and rates: Clay Minerals, v. 39, p. 233–266, https://doi.org/10.1180/0009855043930133.

Image Analysis / Method Summary:

The backscatter electron (BSE) mosaic formed the basis of a detailed analysis of the SSMPs. Some SEM images are composed of 50% BSE and 50% SE signal (Fig. 2). In BSE images, porosity appears black.

To quantify volumes and examine the shape of the SSMPs non-invasive, high-quality, high-resolution synchrotron X-radiation microtomography data of the ultramylonite and its protolith were collected. These datasets were produced with the monochromatic x-ray beam at the

346 TOMCAT beamline of the Swiss Light Source. The samples were mounted onto a rotary stage,
347 where data was collected in 0.25° increments over 180°. The minimum effective pixel size
348 achieved was 0.65 µm to give 0.65 x 0.65 x 0.65 µm3 voxels for three-dimensional rendering of
349 volumes. Virtual representations of the samples were reconstructed from the image projections
350 using gridrec implemented in TOMCAT's in-house reconstruction workflow. The adsorption
351 microtomographic data resolve the different minerals in the sample well and clearly highlight the
352 pores, which attenuate the least and appear darkest in the microtomographs.
353 Porosity in both datasets was segmented using a random forest classifier implemented in the
354 WEKA segmentation tool in FIJI. The resulting probability maps were thresholded to a
355 probability of 80% to account for uncertainties in voxel resolution. Segmented pores were
356 labelled in AVIZO. Labelled pores were visualised in AVIZO (Fig. 3). Before analysing pore
357 size, shape, orientation and location with respect to host clast, the data were binned to achieve a
358 pixel size of 1.3 µm to give 1.3 x 1.3 x 1.3 μm^3 voxels and reduce the noise in the data. A total of
359 73 Ab1 SSMPs, with volumes over 6591 µm3 (3000 voxels) were identified for further analysis.
360

361 EDX analyses of minerals in the matrix and pores are compiled in **Supplementary Dataset 1**.
362

363 **Supplementary figures 1-3**
364 Suppl. Fig. 1 The non-sheared protolith to the ultramylonites investigated in this study. The
365 image shows a virtual slice through a µCT dataset, grey values correspond to x-ray attenuation.
366 The sample (CC12B) was collected just above the shear zone shown in Fig. 1b.
367

Suppl. Fig. 2 Electron images of Ab1 porphyroclasts of different morphologies and their associated SSMPs. a-c) Backscatter electron images, d) Combined (50/50) backscatter/secondary electron image. Scale bar applies to all images.

Suppl. Fig. 3 Aspect ratio, orientation and clast lengths ata from albite porphyroclasts in the undeformed metapsammite (a, b) and its mylonitised counterpart, which exhibits the SSMPs (c-e). In both cases, 73 clasts have been analysed.

Supplementary videos S1-4

Video S1 https://youtu.be/3s_fv-zFGUo This video shows an image slice that is migrating through our µCT volume. The image shows the x-ray attenuation of the least-attenuating voxel for each XY position along a 9.75 µm long ray path orthogonal to the image plane. This technique is excellently suited to highlight porosity in the sample, which appears black.

Video S2 https://youtu.be/R5Y7HFaRlYU This video shows a thick slice that migrates through a subvolume from a µCT dataset collected from an ultramylonite from the Cap de Creus, NE Spain. Pores have been segmented and labelled - individual pores are colour-coded, and only pores larger than 824 µm³ are shown. Note how pores occupy strain shadows around albite porphyroclasts. As the slide moves backwards through the volume, you see pores disappear that "fall out of" the thick slice at the front.

Video S3 https://youtu.be/AU2UeNvnMGw This video shows a thick slice that migrates through a subvolume from a µCT dataset collected from an ultramylonite from the Cap de Creus, NE

Spain. Pores have been segmented and labelled - individual pores are colour-coded, and only pores larger than 824 µm³ are shown. Note how pores occupy strain shadows around albite porphyroclasts. As the slide moves backwards through the volume, you see pores disappear that "fall out of" the thick slice at the front.

Video S4 https://youtu.be/2j1sJDI8CYg This video shows a subvolume from a µCT dataset collected from an ultramylonite from the Cap de Creus, NE Spain. Pores have been segmented and labelled - individual pores are colour-coded, and only pores larger than 824 µm³ are shown. Note how pores occupy strain shadows around albite porphyroclasts.

Please visit https://doi.org/10.1130/XXXX to access the supplemental material, and contact editing@geosociety.org with any questions.

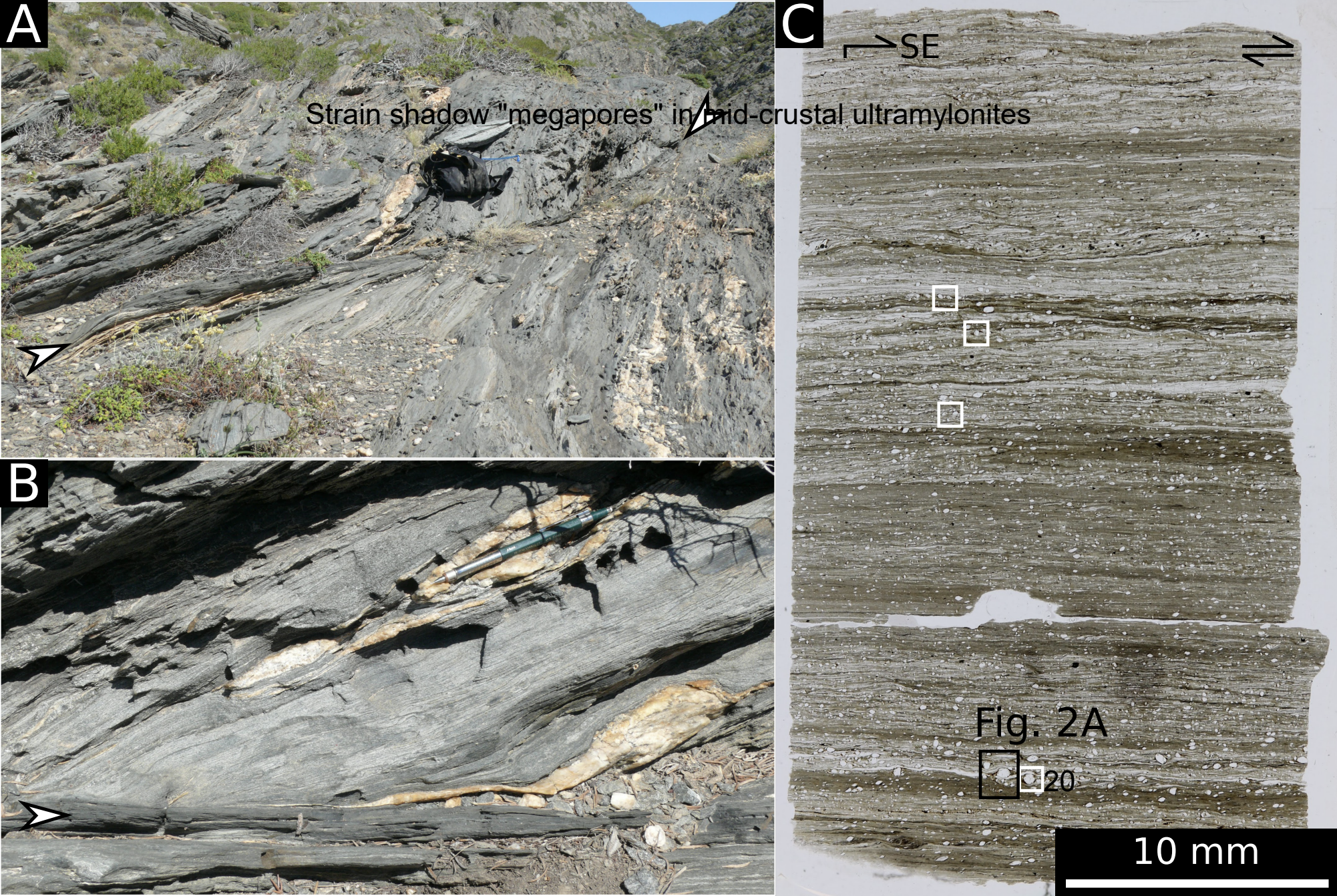
A
Strain shadow "megapores" in mid-crustal ultramylonites
B
C
SE
Fig. 2A
20
10 mm

Strain shadow "[illegible]ores" in mid-crustal ultramylonites

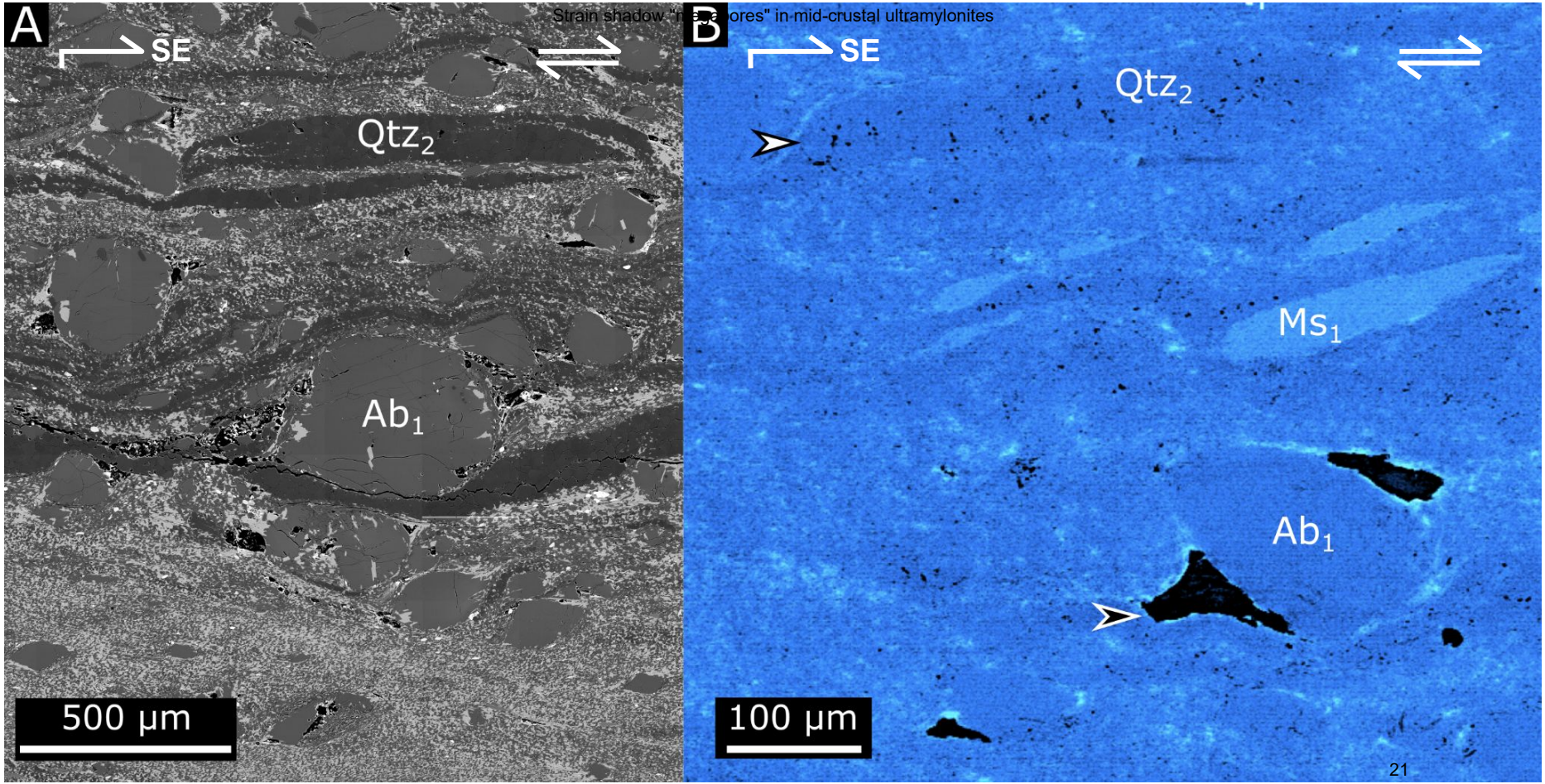

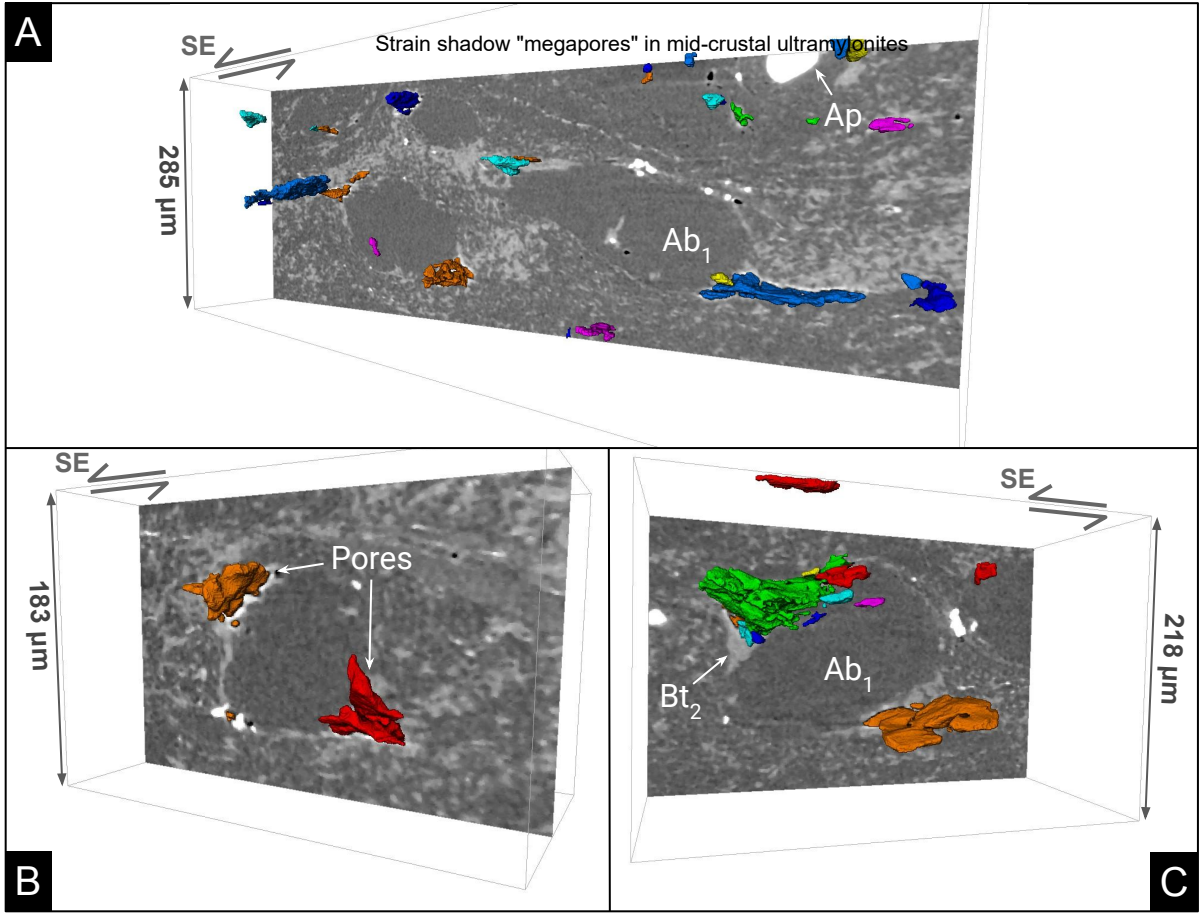
A
SE
Strain shadow "megapores" in mid-crustal ultramylonites
285 µm
Ap
Ab1
B
SE
183 µm
Pores
C
SE
218 µm
Ab1
Bt2

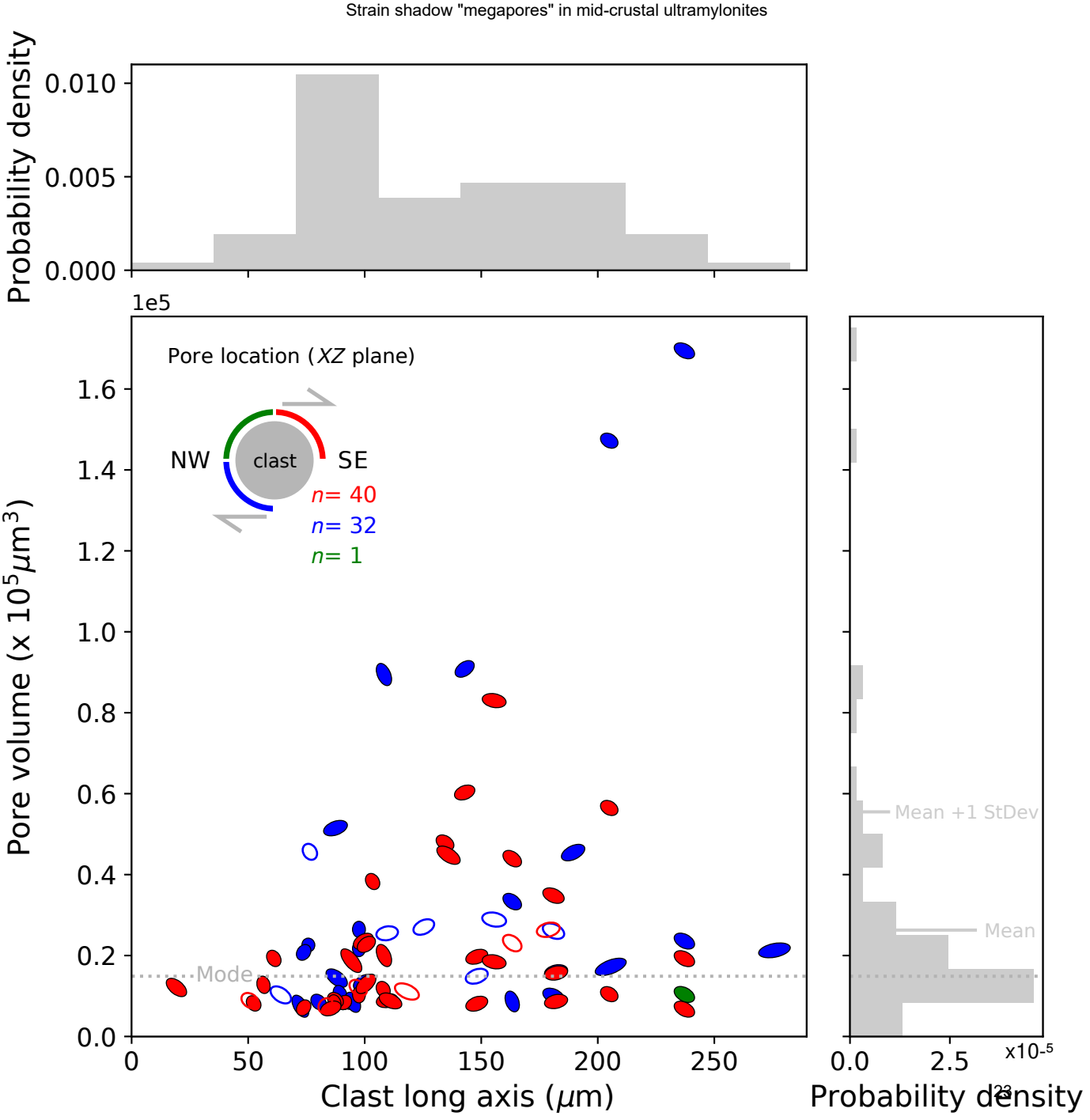
Strain shadow "megapores" in mid-crustal ultramylonites
Probability density
0.010
0.005
0.000
1e5
Pore location (XZ plane)
NW
clast
SE
n= 40
n= 32
n= 1
Pore volume (x 10^5 μm^3)
1.6
1.4
1.2
1.0
0.8
0.6
0.4
0.2
0.0
Mode
0
50
100
150
200
250
Clast long axis (μm)
Mean +1 StDev
Mean
0.0
2.5
x10-5
Probability density

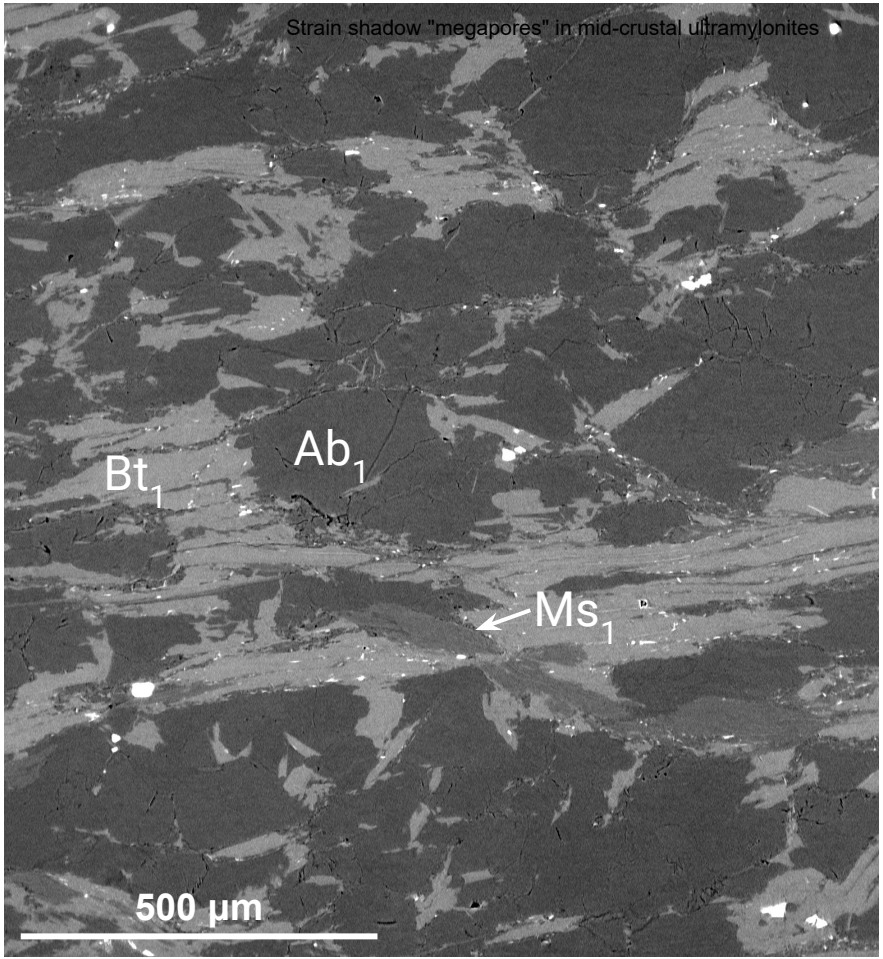
Strain shadow "megapores" in mid-crustal ultramylonites
Bt1
Ab1
Ms1
500 µm

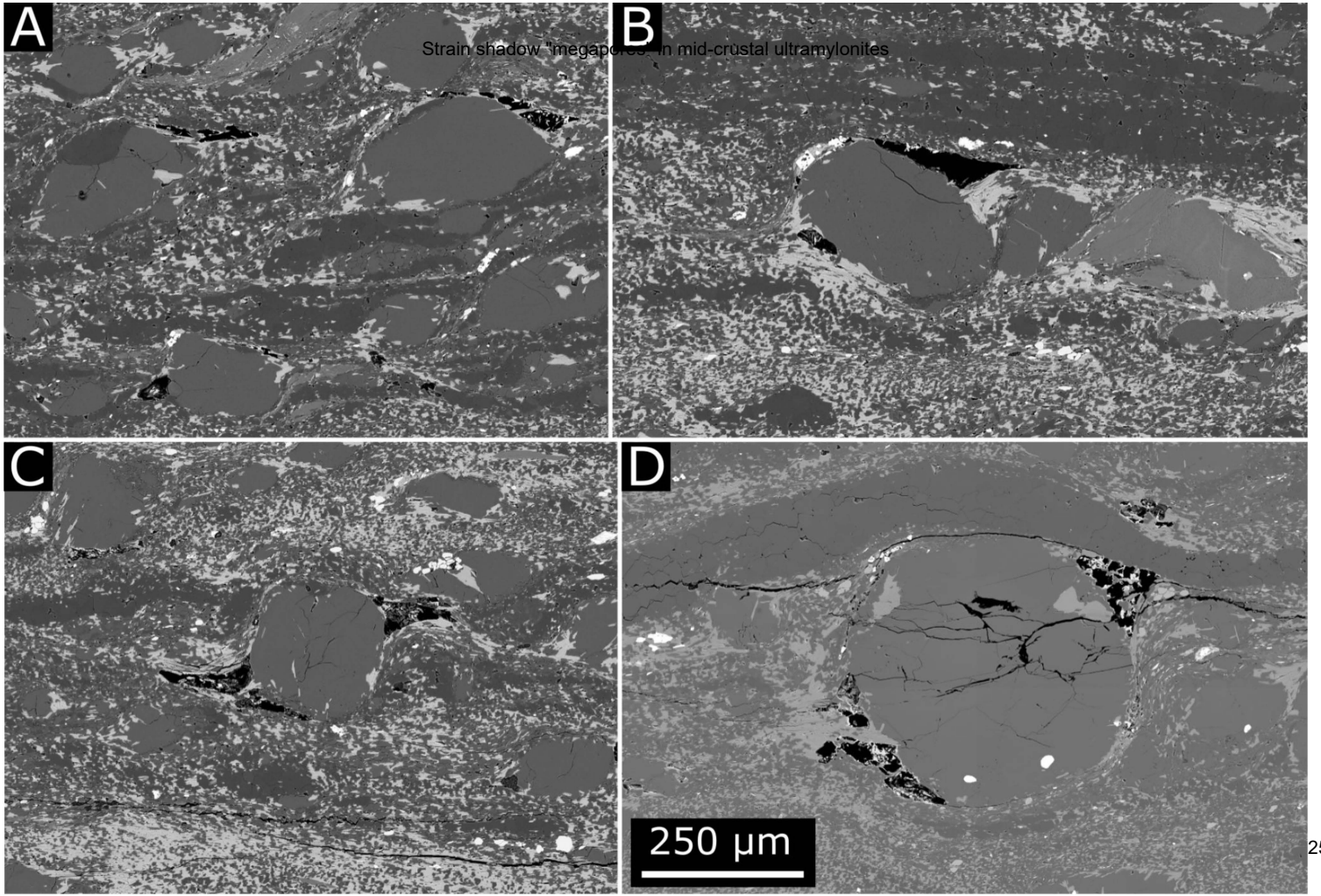

Strain shadow "megapores" in mid-crustal ultramylonites

Strain shadow "megapores" in mid-crustal ultramylonites